Int. J. Heat Mass Transfer. Vol. 25, No. 11, pp. 1677–1687, 1982
Printed in Great Britain

0017–9310/82/111677–11 $03.00/0
Pergamon Press Ltd.

NUMERICAL SIMULATION OF FREE CONVECTIVE HEAT TRANSFER FROM A SPHERE

F. GEOOLA
Materials and Energy Research Centre (MERC), P.O. Box 41-2927, Tehran, Iran

and

A. R. H. CORNISH
Chemical Engineering Department, Imperial College of Science and Technology, Prince Consort Rd., London S.W.7, U.K.

(*Received* 23 *September* 1981 *and in revised form* 8 *March* 1982)

Abstract—A numerical study of time-dependent free convective heat transfer from a solid sphere to an incompressible Newtonian fluid has been carried out for Grashof numbers between 0.05 and 12 500 and for Prandtl numbers of 0.72, 10 and 100. The energy and vorticity transport equations were solved using Peaceman and Rachford's ADI method and the stream function equation was solved using point iterative successive over-relaxation. From the late-time steady-state solutions it was observed that even at extremely low Grashof numbers, weak convection processes were present in the region close to the outer boundary. However, it was found that even at moderate Grashof numbers the dominant mode of vorticity transport close to the surface was by diffusion.

NOMENCLATURE

C_{DF}, dimensionless viscous drag;
C_{DP}, dimensionless pressure drag;
C_{DT}, dimensionless total drag;
C_p, specific heat at constant pressure;
G, modified dimensionless vorticity, defined by equation (6);
Gr, Grashof number based on the radius of the sphere, $[R^3\beta g(T_s - T_\infty)]/\nu^2$;
g, gravitational acceleration;
h, average heat transfer coefficient;
h_θ, local heat transfer coefficient;
K_0, dimensionless pressure at the front stagnation point;
K_θ, dimensionless pressure at sphere surface;
k, thermal conductivity;
M, number of mesh points in the z direction;
m, mesh size in the z direction;
N, number of mesh points in the θ direction;
n, mesh size in the θ direction;
Nu, average Nusselt number, $(2Rh)/k$;
Nu_θ, local Nusselt number, $(2Rh_\theta)/k$;
Pr, Prandtl number, ν/α;
R, radius of sphere;
Ra, Rayleigh number, $GrPr$;
r, dimensionless radial coordinate;
(r, θ, ϕ), spherical polar coordinates;
T, dimensionless temperature;
t, dimensionless time;
u_z, u_θ, dimensionless velocity components in the z and θ directions;
y_1, y_2, y_3, rectangular cartesian coordinates;
z, modified coordinate defined as $z = \ln r$.

Greek symbols

α, thermal diffusivity, $k/(\rho C_p)$;
β, volumetric coefficient of expansion with temperature;
Δt, dimensionless time-step;
ε_ψ, convergence criterion for the stream function;
ζ, dimensionless vorticity component in the ϕ direction;
θ, angular coordinate;
ν, fluid kinematic viscosity;
ρ, density;
ϕ, coordinate representing the angle of rotation about the axis of symmetry of the flow;
ψ, dimensionless stream function;
ω_z, weighting factor for upwind difference representation of a first order derivative with respect to z;
ω_θ, weighting factor for upwind difference representation of a first order derivative with respect to θ;
ω_ψ, relaxation factor for the stream function.

Subscripts

i, mesh point index in the z direction;
j, mesh point index in the θ direction;
i, j, indices of a mesh point in the flow region;
s, sphere surface;
∞, outer boundary condition.

Superscripts

(L), (L)th iteration;
$(L+1)$, $(L+1)$th iteration;

p, pth time-step;
$p + 1/2$, $(p + 1/2)$th time-step;
$p + 1$, $(p + 1)$th time-step.

1. INTRODUCTION

THE PROCESSES of heat and mass transfer by free convection from particles to fluids are of importance industrially in connection with combustion, vaporization, drying, performance of packed catalytic reactors, etc. Furthermore, because of the complexity of multiparticle systems in theoretical studies, a single solid sphere, liquid drop or gas bubble is usually studied in order to understand the fundamental aspects of transfer mechanisms. The solid sphere is the most common unit for these studies and the results are valuable in the absence of results for multiparticle systems.

The pertinent analytical and experimental studies of time-independent free convective heat transfer from a sphere at low and moderate Grashof numbers ($Gr \leqslant 10^5$) which have been reported include analytical studies [1, 2], analytical and experimental work [3], and experimental works [4–9]. In most of the investigations only the average Nusselt numbers were determined, only one [3] obtaining flow patterns and temperature distributions about a sphere and then only for extremely small Grashof numbers ($Gr \leqslant 1.0$). In a recent paper [10] the present authors gave complete numerical solutions for time-independent free convective heat transfer from a solid sphere in the range of Grashof number between 0.05 and 50 by application of an extrapolated Gauss–Seidel method. However, it was observed that the method used could not be applied to find solutions for Grashof numbers greater than 50. There have been no reports of complete analytical or numerical solutions of time-dependent or time-independent free convective heat transfer from a solid sphere for Grashof numbers larger than 50.

In the present study, the time-dependent Navier–Stokes equation for axisymmetric free convection from a sphere and the continuity equation were combined and expressed as a vorticity transport equation and a stream function equation. These latter two and the energy equation were solved numerically and simultaneously using an upwind differencing scheme applied to the convective terms of the transport equations. The time-dependent vorticity transport and energy equations were solved using Peaceman and Rachford's alternating direction implicit, (ADI), method [11]. The stream function equation was solved using a point iterative successive over-relaxation method.

2. MATHEMATICAL MODEL

The mathematical model consists of a set of differential equations and initial and boundary conditions describing time-dependent free convective heat transfer from a heated solid sphere which is immersed in a stagnant Newtonian medium and enclosed by a concentric spherical shell of uniform and unchanging temperature.

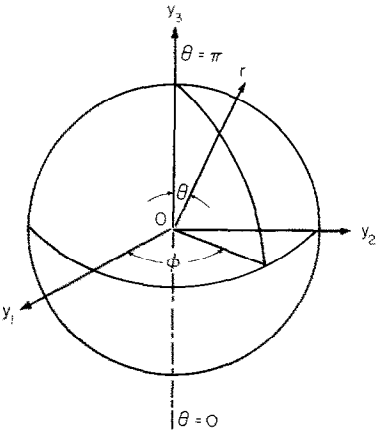

FIG. 1. Spherical polar coordinate system.

To simulate the flow around a solid sphere, the time-dependent Navier–Stokes, energy and continuity equations were expressed in spherical polar coordinates. The spherical polar coordinates of the sphere are arranged as shown in Fig. 1. As shown in the figure, the coordinate r is normal to the surface of the body, θ is parallel to the surface in the flow direction and ϕ is the direction of rotation about the axis of symmetry of the flow. For the particular case of streaming flow past a stationary sphere with no rotation, the flow around the vertical axis is axisymmetric, the component of velocity in the ϕ direction is zero everywhere, and all variables are independent of ϕ.

The time-dependent Navier–Stokes and the continuity equations were combined and expressed as a time-dependent vorticity transport and a stream function equation set. The derivation of this equation set may be found elsewhere [12]. From the definition of the vorticity vector [12] and from the condition of axisymmetrical flow, there is only one non-zero component of vorticity, that is in the ϕ direction. In derivation of the equations it is assumed that the only body force operating is that of gravity and that temperature variations within the fluid are not large, so that Boussinesq's approximation can be applied thus enabling the density to be treated as a constant in all terms of the transport equations except the buoyancy term. For the same reason, other fluid properties such as viscosity, specific heat, and thermal conductivity are considered to be constant.

For ease of obtaining numerical solutions of the equations, the variables have been rendered dimensionless with respect to the radius of the sphere, the kinematic viscosity of the fluid at the temperature of the outer boundary, and the temperature difference between the sphere surface and the outer boundary. It was also convenient to transform the equations from polar coordinates (r, θ) to rectangular coordinates (z, θ) by means of the transformation of $r = e^z$.

With the above considerations the resulting system of dimensionless equations in rectangular coordinates (z, θ) can be written as follows:

The velocity components

$$u_z = -\frac{1}{e^{2z}\sin\theta}\frac{\partial\psi}{\partial\theta}, \tag{1}$$

$$u_\theta = \frac{1}{e^{2z}\sin\theta}\frac{\partial\psi}{\partial z}. \tag{2}$$

The energy equation

$$e^{2z}\frac{\partial T}{\partial t} + \frac{1}{e^{z}\sin\theta}\left(\frac{\partial\psi}{\partial z}\frac{\partial T}{\partial\theta} - \frac{\partial\psi}{\partial\theta}\frac{\partial T}{\partial z}\right) = \frac{1}{Pr}\left(\frac{\partial^2 T}{\partial z^2} + \frac{\partial T}{\partial z} + \frac{\partial^2 T}{\partial\theta^2} + \cot\theta\frac{\partial T}{\partial\theta}\right). \tag{3}$$

The vorticity transport equation

$$e^{2z}\frac{\partial G}{\partial t} + \frac{1}{e^{z}\sin\theta}\left[\frac{\partial\psi}{\partial z}\left(\frac{\partial G}{\partial\theta} - 2\cot\theta G\right) - \frac{\partial\psi}{\partial\theta}\left(\frac{\partial G}{\partial z} - 2G\right)\right] = e^{2z}E^2(G) + e^{2z}\sin^2\theta\, Gr\left(\frac{\partial T}{\partial z} + \cot\theta\frac{\partial T}{\partial\theta}\right). \tag{4}$$

The stream function equation

$$e^{2z}G = e^{2z}E^2(\psi) \tag{5}$$

where

$$G = \zeta e^{z}\sin\theta \tag{6}$$

and

$$e^{2z}E^2 = \frac{\partial^2}{\partial z^2} - \frac{\partial}{\partial z} + \frac{\partial^2}{\partial\theta^2} - \cot\theta\frac{\partial}{\partial\theta}. \tag{7}$$

Equations (1)–(7) together with the following boundary and initial conditions were solved numerically:

Sphere surface: at $z = 0$ for $0 \leqslant \theta \leqslant \pi$, $t \geqslant 0$.

$$\psi = 0,\ \frac{\partial\psi}{\partial z} = 0,\ \frac{\partial\psi}{\partial\theta} = 0,\ \frac{\partial^2\psi}{\partial\theta^2} = 0, \tag{8}$$

$$G = \zeta\sin\theta = \frac{\partial^2\psi}{\partial z^2},\quad T = 1.$$

Axis of symmetry: at $\theta = 0$ and $\theta = \pi$ for all values of z, $t \geqslant 0$.

$$\psi = 0;\ \frac{\partial\psi}{\partial z} = 0;\ \frac{\partial^2\psi}{\partial z^2} = 0;\ \frac{\partial\psi}{\partial\theta} = 0, \tag{9}$$

$$G = 0;\ \zeta = 0;\ \frac{\partial T}{\partial\theta} = 0.$$

Outer boundary. At large distances away from the sphere surface, the dependent variables become asymptotic to their values in the undisturbed stagnant fluid. Mathematically, the conditions at this boundary are well defined as z tends to infinity. However, because of limitations on computer storage and computation time, numerical integration cannot be made over too large a region, and a finite domain of integration has to be used. Therefore, the outer boundary condition was applied at some finite distance from the sphere surface. The conditions at the outer boundary can be expressed as

$$\text{At } z = z_\infty \text{ for } 0 \leqslant \theta \leqslant \pi,\ t \geqslant 0,\quad \psi = 0,\quad G = 0,\quad \zeta = 0,\quad T = 0. \tag{10}$$

The initial conditions were as follows: at $t = 0$ for $0 \leqslant z \leqslant z_\infty$, $0 \leqslant \theta \leqslant \pi$:

$$\psi = 0,\quad \zeta = 0,\quad G = 0,\quad T = T^0. \tag{11}$$

The initial temperature distribution, T^0, was taken to be that of pure radial steady-state conduction between the sphere and the surrounding fluid, that is

$$T^0 = \left[\frac{e^{z_\infty}}{(e^{z_\infty} - 1)}\right]e^{-z} - \left[\frac{1}{(e^{z_\infty} - 1)}\right]. \tag{12}$$

From the distribution of stream function, vorticity and temperature other quantities were calculated as follows:

Local Nusselt number.

$$Nu = -2\left.\frac{\partial T}{\partial z}\right|_{z=0}. \tag{13}$$

Average Nusselt number.

$$Nu = 1/2\int_0^\pi Nu_\theta\sin\theta\,d\theta. \tag{14}$$

Dimensionless pressure at the front stagnation point.

$$K_0 = 4\int_0^{z_\infty}\frac{\partial\zeta}{\partial\theta}dz - 2\int_0^{z_\infty}\frac{1}{e^{z}}\frac{\partial}{\partial t}\left(\frac{\partial^2\psi}{\partial\theta^2}\right)dz + 2Gr\int_0^{z_\infty} Te^{z}\,dz. \tag{15}$$

Dimensionless pressure at the sphere surface (surface pressure).

$$K_\theta = K_0 + 2Gr(1 - \cos\theta) + 2\int_0^\theta\left(\frac{\partial\zeta}{\partial z} + \zeta\right)d\theta. \tag{16}$$

Dimensionless pressure drag (pressure drag coefficient)

$$C_{DP} = \int_0^\pi K_\theta\sin 2\theta d\theta. \tag{17}$$

Dimensionless viscous drag (viscous drag coefficient).

$$C_{DF} = 4\int_0^\pi \zeta_s\sin^2\theta d\theta. \tag{18}$$

Dimensionless total drag (total drag coefficient).

$$C_{DT} = C_{DP} + C_{DF}. \tag{19}$$

The integrands in equations (15) and (16) were

evaluated at $\theta = 0$ and at $z = 0$, respectively. For a detailed analysis of this section see ref. [13].

3. NUMERICAL METHOD

The set of partial differential equations, energy equation (3), vorticity transport equation (4) and stream function equation (5), presented in Section 2, is non-linear second order elliptic with respect to the space variables (z, θ). Also equations (3) and (4) are parabolic with respect to time. These equations together with the associated boundary and initial conditions given in Section 2 were solved numerically.

The first step in obtaining a numerical solution of partial differential equations is to formulate the original equations as finite-difference equations. Basically, the domain over which the equations are to be integrated, the flow region, is presented by a finite number of points or nodes spaced systematically in the domain. This is followed by a discretization process which is normally carried out using a Taylor's series expansion of a function about a general node and relating the value of function at that node to those at neighbouring nodes. In the present study a five point approximation, involving four neighbouring points, has been used and the mesh points were spaced uniformly in both the z and θ directions. The details of the method used can be found elsewhere [14–16].

The time-dependent vorticity transport and energy equations were solved using Peaceman and Rachford's alternating direction implicit, (ADI), method [11]. The ADI method makes use of a splitting of the time-step to obtain a multi-dimensional implicit method which requires only the inversion of a tridiagonal matrix. Roache [16] has given a survey of the early applications of the ADI method to fluid dynamics problems. In addition to the works surveyed [16], other solutions obtained [17–19] support the suitability of Peaceman and Rachford's ADI method for solving the vorticity transport and energy equations for flow around objects [16].

In order to preserve the 'transportive property' [16] and to obtain rapid convergence, an upwind differencing method was used for the finite-difference representation of the convective terms of the vorticity transport and energy equations. A detailed analysis of the application of the upwind differencing method for the finite-difference representation of convective terms of equations is given in ref. [10]. There are many arguments for and against the application of upwind differencing method (e.g. [16, 18, 20, 21]). However, the solutions obtained by other authors (as surveyed [16]) for multi-dimensional problems support the use of upwind difference scheme.

As an example of the scheme used, the finite-difference approximations of the vorticity transport equation when expended into sets of simultaneous equations for the time-step p to $(p + 1/2)$, in the θ direction, can be written as follows:

$$C_{1j} G^{p+1/2}_{i,j-1} + C_{2j} G^{p+1/2}_{i,j} + C_{3j} G^{p+1/2}_{i,j+1} = D^p_j \quad (20)$$

where

$$D^p_j = C_{1i} G^p_{i-1,j} + C_{2i} G^p_{i,j} + C_{3i} G^p_{i+1,j} + C_{4ij}. \quad (21)$$

Similarly, the finite-difference approximation of the vorticity transport equation when expanded into sets of simultaneous equations for the time-step $p + 1/2$ to $p + 1$, in the z direction, is as follows:

$$C'_{1i} G^{p+1}_{i-1,j} + C'_{2i} G^{p+1}_{i,j} + C'_{3i} G^{p+1}_{i+1,j} = D^{p+1/2}_i \quad (22)$$

where

$$D^{p+1/2}_i = C'_{1j} G^{p+1/2}_{i,j-1} + C'_{2j} G^{p+1/2}_{i,j} + C'_{3j} G^{p+1/2}_{i,j+1} + C_{4ij}. \quad (23)$$

The coefficients of equations (20)–(23) for backward, forward and central differences (ω_θ or $\omega_z = 0$, ω_θ or $\omega_z = 1$ and ω_θ or $\omega_z = 0.5$, respectively) may be expressed as follows:

$$C_{1j} = -b_{4j} - KG_{ij}\Delta_i(\psi_{ij})(1 - \omega_\theta), \quad (24)$$

$$C_{2j} = \frac{1}{X_i} + \frac{2}{an^2} + KG_{ij}\Delta_i(\psi_{ij}) \times (1 - 2\omega_\theta - 2n\cot\theta_j), \quad (25)$$

$$C_{3j} = -b_{3j} + KG_{ij}\Delta_i(\psi_{ij})\omega_\theta, \quad (26)$$

$$C_{1i} = b_{2i} - KG_{ij}\Delta_j(\psi_{ij})(1 - \omega_z), \quad (27)$$

$$C_{2i} = \frac{1}{X_i} - \frac{2}{am^2} + KG_{ij}\Delta_j(\psi_{ij})(1 - 2\omega_z - 2m), \quad (28)$$

$$C_{3i} = b_{1i} + KG_{ij}\Delta_j(\psi_{ij})\omega_z, \quad (29)$$

$$C'_{1j} = -C_{1j}, \quad (30)$$

$$C'_{2j} = -C_{2j} + \frac{2}{X_i}, \quad (31)$$

$$C'_{3j} = -C_{3j}, \quad (32)$$

$$C'_{1i} = -C_{1i}, \quad (33)$$

$$C'_{2i} = -C_{2i} + \frac{2}{X_i}, \quad (34)$$

$$C'_{3i} = -C_{3i}, \quad (35)$$

$$C_{4ij} = \frac{e^{2z_i}\sin^2\theta_j Gr}{2mn}[n(T_{i+1,j} - T_{i-1,j}) + m\cot\theta_j(T_{i,j+1} - T_{i,j-1})] \quad (36)$$

where

$$b_{1i} = \frac{1}{a}\left(\frac{1}{m^2} - \frac{1}{2m}\right), \quad (37)$$

$$b_{2i} = \frac{1}{a}\left(\frac{1}{m^2} + \frac{1}{2m}\right), \quad (38)$$

$$b_{3j} = \frac{1}{a}\left(\frac{1}{n^2} - \frac{\cot\theta_j}{2n}\right), \quad (39)$$

$$b_{4j} = \frac{1}{a}\left(\frac{1}{n^2} + \frac{\cot\theta_j}{2n}\right), \quad (40)$$

$$a = \frac{2}{m^2} + \frac{2}{n^2}, \tag{41}$$

$$X_i = \frac{a\Delta t}{2e^{2z_i}}, \tag{42}$$

$$KG_{ij} = \frac{e^{z_i} \sin \theta_j}{2amn}, \tag{43}$$

$$\Delta_i(\psi_{ij}) = \psi_{i+1,j} - \psi_{i-1,j}, \tag{44}$$

$$\Delta_j(\psi_{ij}) = \psi_{i,j+1} - \psi_{i,j-1}. \tag{45}$$

In the calculation of the variable coefficients (24)–(36), the most up to date values of the relevant variables are used.

The sets of simultaneous algebraic equations, [such as equations (20) and (22)], obtained by the finite-difference representation of the vorticity transport and energy equations, were solved using Thomas's elimination method [22].

In the present work the stream function equation, equation (5), was solved at any time-step using a point iterative successive over-relaxation method [16]. By the use of the coefficients (37)–(41), equation (5) was expanded as follows:

$$\psi^p_{i,j} = b_{1i}\psi^p_{i+1,j} + b_{2i}\psi^p_{i-1,j} + b_{3j}\psi^p_{i,j+1} + b_{4j}\psi^p_{i,j-1} - C_i G^p_{i,j} \tag{46}$$

where

$$C_i = \frac{e^{2z_i}}{a}. \tag{47}$$

A relaxation factor, ω_ψ, was defined as follows:

$$\psi^{p,(L+1)}_{i,j} = \psi^{p,(L)}_{i,j} + \omega_\psi(\psi^p_{i,j} - \psi^{p,(L)}_{i,j}) \tag{48}$$

where the contour (L) refers to the number of successive point iterations performed at the pth time-step, and $\psi^{p,(L+1)}_{i,j}$ is the value of the stream function at the pth time-step after $(L+1)$ iterations. The stream function values, $\psi^{p,(L+1)}_{i,j}$, are resubstituted into equation (46) which is then resolved with equation (48) until the following convergence criterion is satisfied:

$$|\psi^{p,(L+1)}_{i,j} - \psi^{p,(L)}_{i,j}| \leqslant \varepsilon_\psi. \tag{49}$$

The numerical integration in equations (13)–(19) were carried out using the trapezoidal rule [23]. The gradients involved in equations (13)–(19) and in the boundary conditions were evaluated by fitting appropriate polynomials to the calculated values at the neighbouring nodes [13].

A computer program was developed to solve the finite-difference equations. The solutions were obtained in the form of distributions of temperature, vorticity and stream function and were used to calculate the other quantities required such as local and average Nusselt numbers, the pressure distribution on the surface of the sphere, and the viscous, pressure, and total drag coefficients. The average central processor time required to obtain a late-time steady-state solution was found to be approximately 3.5 h when using a CDC-7600 digital computer. However, as was stated earlier the solutions obtained are thought to be of general interest in a wide number of practical applications.

It will be seen in this paper that the late-time steady-state values obtained for the average Nusselt number were found to agree reasonably well with those obtained experimentally by other workers. However, no experimental data are available for comparison with other results obtained in the present work such as the distributions of surface vorticity, surface pressure and the viscous, pressure, and total drag coefficients. As a check on the accuracy of the numerical solutions in the absence of sufficient experimental data the following derivatives were calculated from the solutions: the first order derivative of temperature with respect to θ along the axis of symmetry; the first order derivatives of the stream function along the surface of the sphere and the axis of symmetry with respect to θ and z; and the first order derivative of vorticity with respect to θ along the axis of symmetry. For all the solutions, the values of the above derivatives were calculated and found to have a magnitude of 10^{-10}–10^{-20} which was sufficiently close to the required value of zero.

The accuracy of the results obtained and the economy of the procedure used, like any other finite-difference method [21], were mainly dependent on the mesh sizes, magnitude of the time-step, position of the outer boundary, orders of the polynomials used to approximate the boundary conditions, convergence criteria, and associated relaxation factors. Values for these factors were found on the basis of numerical experiments and were selected in order to achieve convergence while keeping a balance between accuracy of the solutions, as far as it could be assessed, and economy of use of computing facilities.

In the present work, the values of the constants m, n, M and N for all Grashof numbers except a Grashof number of 12 500 were set equal to 0.04, 6°, 80 and 30, respectively. However, for a Grashof number of 12 500 the values were set equal to 0.04, 6°, 60 and 30, respectively.

The values of the time-steps, relaxation factors and convergence criteria for different Grashof numbers are presented in Table 1.

For a detailed analysis of this section see ref. [13].

4. DISCUSSION OF RESULTS

The characteristics displayed by the solutions were broadly similar and differed only in detail. Thus, only one solution will be discussed fully; that for a Grashof number of 25 and a Prandtl number of 0.72. This solution is particularly chosen since its result can be compared with the result presented in ref. [10] (for other solutions see ref. [13]).

The numerical results are presented in terms of dimensionless variables. For the solution being considered, the late-time steady-state condition was attained at a dimensionless time of 2.16.

Table 1. Main results of the present study as the solutions of the time-dependent equations approach late-time steady-state

Gr	Pr	Δt	ε_ψ	ω_ψ	Nu	K_0	K_π	C_{DF}	C_{DP}
0.05	0.72	0.01	10^{-6}	1.9	2.09	0.49	−0.49	1.13	0.59
1	0.72	0.01	10^{-6}	1.6	2.34	6.32	−5.69	15.75	7.95
10	0.72	0.005	5×10^{-6}	1.5	2.92	37.44	−33.60	78.25	42.36
25	0.72	0.001	7.5×10^{-6}	1.5	3.30	81.59	−46.05	146.39	82.62
50	0.72	0.001	2.5×10^{-5}	1.5	3.82	141.26	−54.43	236.11	138.18
50	100	0.001	2.5×10^{-5}	1.5	8.21	122.6	−57.37	195.04	114.61
125	0.72	0.001	5×10^{-5}	1.5	4.25	297.28	−61.53	448.31	276.20
1250	10	0.0005	10^{-3}	1.5	9.98	1988.35	−71.10	1958.01	1386.11
12500	10	0.00001	2.5×10^{-3}	1.3	16.82	12077.34	3904	8700.77	6606.85

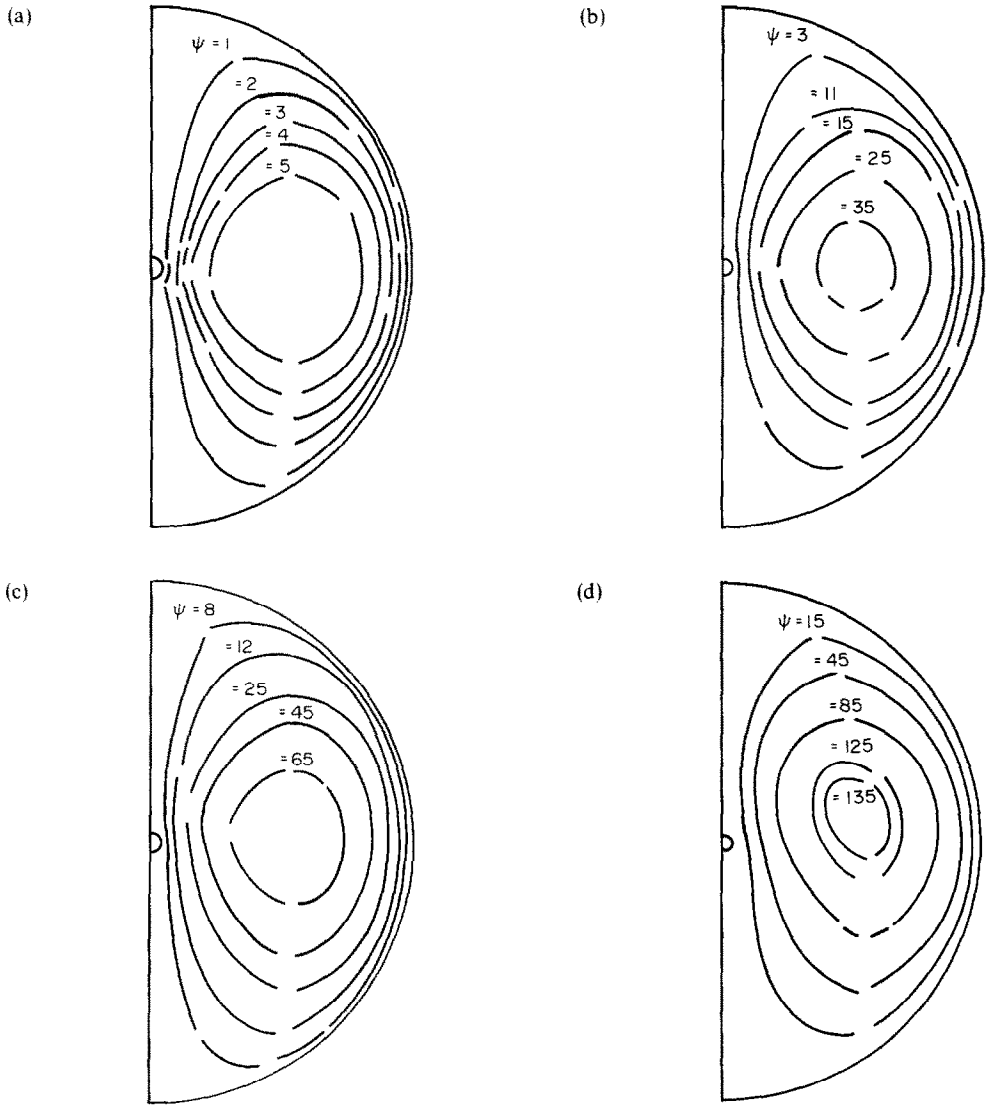

FIG. 2. Development of streamlines with time, $Gr = 25$, $Pr = 0.72$. case (a): $t = 0.1$; case (b): $t = 0.5$; case (c): $t = 1$; case (d): $t = 2.16$.

The development with time of the streamlines starting from a motionless flow field is shown in Fig. 2. The rising and descending currents generate a circulatory flow pattern as shown by the streamlines plotted in Fig. 2. Case (d) of Fig. 2. shows that the streamlines at the late-time steady-state conditions are displaced slightly in the downstream direction as a result of convection effects.

Isotherms around the sphere at various dimensionless times are shown in Fig. 3. During the early stages of simulation, the thickness of the heated region around the solid sphere is almost uniform and heat

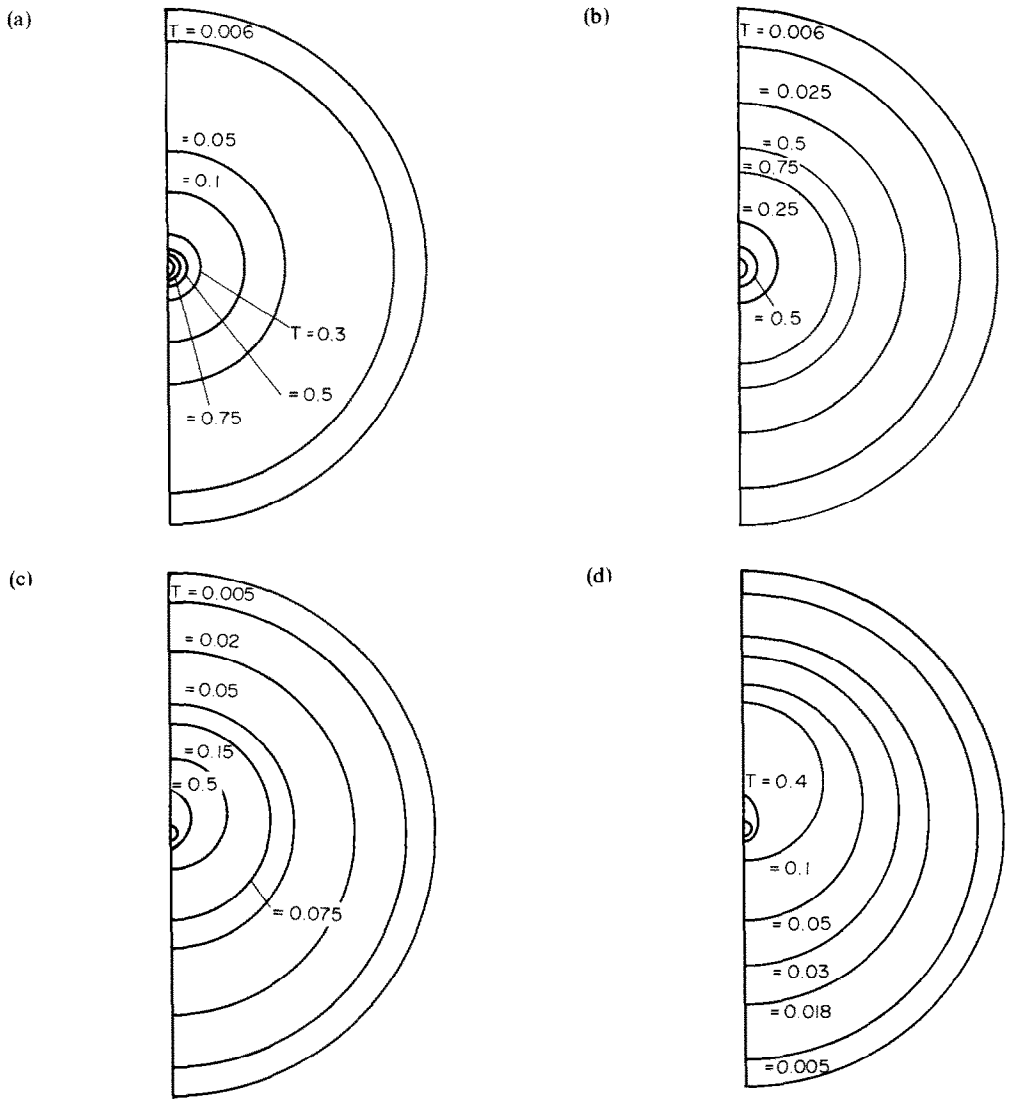

FIG. 3. Development of isotherms with time, $Gr = 25$, $Pr = 0.72$. case (a): $t = 0.1$; case (b): $t = 0.5$; case (c): $t = 1$; case (d): $t = 2.16$.

transfer takes place mainly by unsteady-state conduction. However, as the simulation proceeds, the convective effects increase in magnitude and the isotherms become closer to the surface of the sphere in the upstream region and extend further downstream at the rear of the sphere. Case (d) of Fig. 3 shows the isotherms around the sphere at the late-time steady-state condition.

The generation and development with time of vorticity around the solid sphere can be seen in Fig. 4. During the early stages of simulation, diffusion is the dominant mode of vorticity transport, as shown by case (a) of Fig. 4. However, as time proceeds, the effects of convection on the distribution of vorticity become more important than the effects of diffusion and as can be seen in cases (c) and (d) of Fig. 4, the contours are displaced in the downstream direction.

The behaviour of the drag coefficients with time is shown in Fig. 5. Both the pressure drag and viscous drag coefficients show a smooth increase with time.

Figure 6 shows the variation of the local Nusselt number with time. Since steady-state conduction in a finite space is used as the initial condition, the local Nusselt number starts from a value of 2.085 which is constant around the solid sphere. However, as integration proceeds with time, the convective effects increase so that the local Nusselt numbers over the upstream region of the sphere increase continuously towards their late-time steady-state values while the local Nusselt numbers over the rear part of the sphere first decrease and then increase again to their late-time steady-state values as the circulation within the fluid becomes more vigorous.

The variations of surface pressure and surface vorticity with time are shown in Figs. 7 and 8, respectively. It is seen from Fig. 7 that as time proceeds,

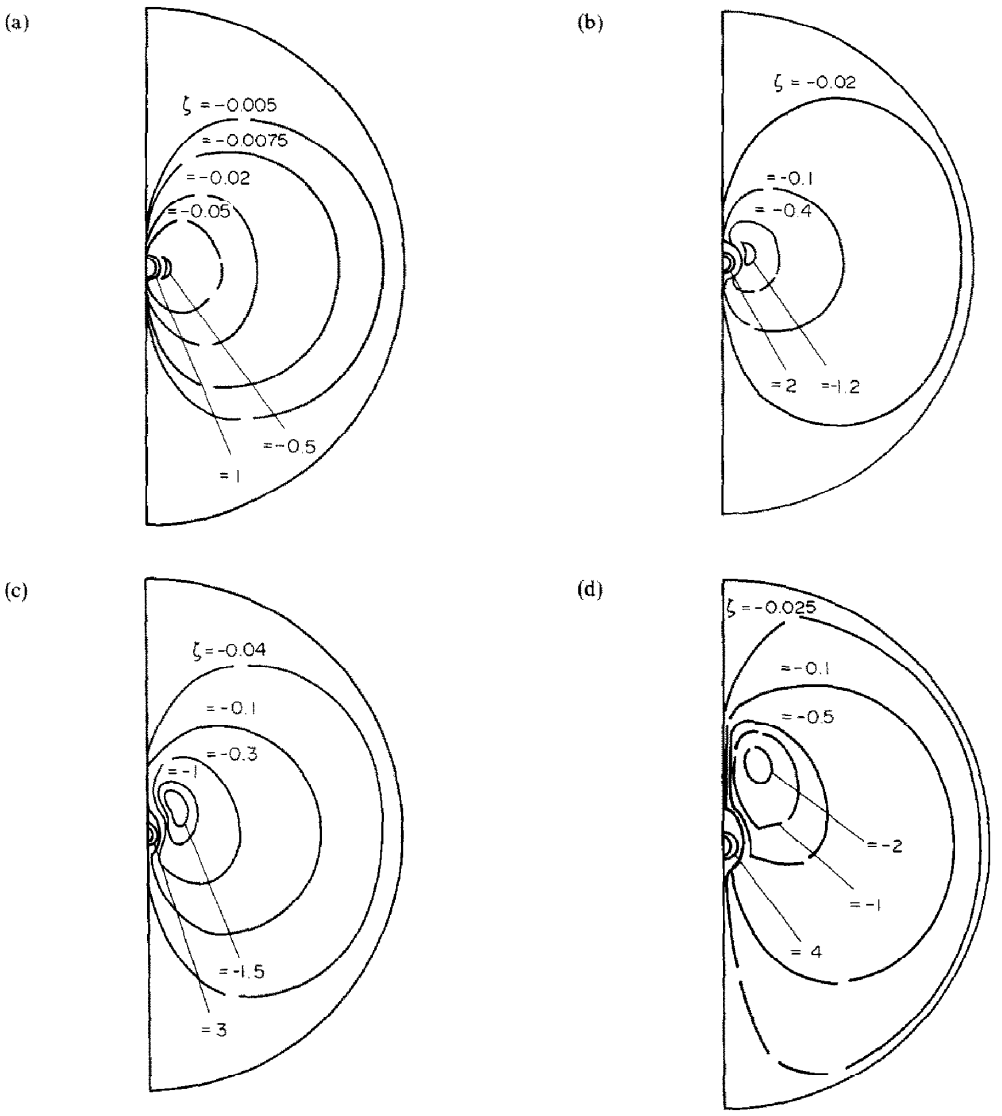

FIG. 4. Development of vorticity with time, $Gr = 25$, $Pr = 0.72$. case (a): $t = 0.1$; case (b): $t = 0.5$; case (c): $t = 1$; case (d): $t = 2.16$.

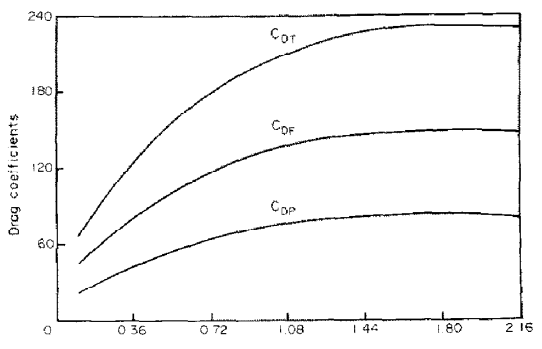

FIG. 5. Drag coefficients vs time, $Gr = 25$, $Pr = 0.72$.

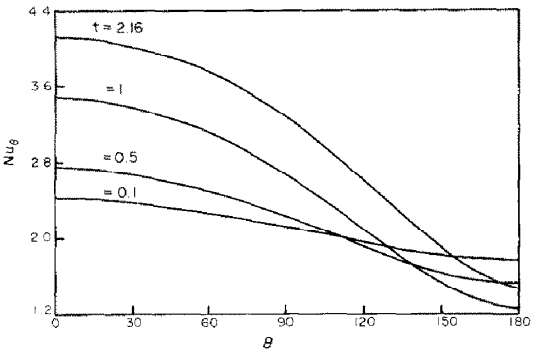

FIG. 6. Local Nusselt number vs time, $Gr = 25$, $Pr = 0.72$.

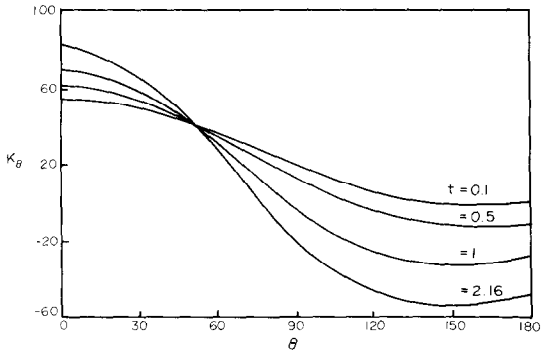

FIG. 7. Surface pressure vs time $Gr = 25$, $Pr = 0.72$.

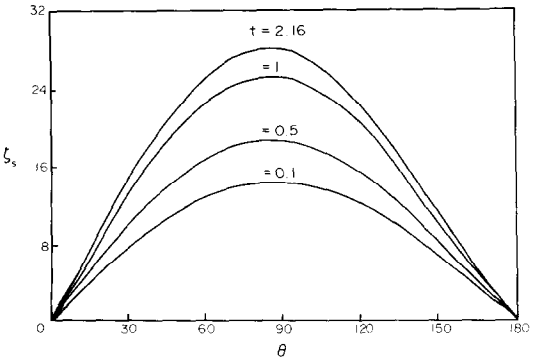

FIG. 8. Surface vorticity vs time, $Gr = 25$, $Pr = 0.72$.

the surface pressure increases in the upstream region and decreases in the downstream region. Figure 8 shows that at Grashof number of 25 and a Prandtl number of 0.72 the dominant mode of vorticity transport very close to the surface is diffusion.

In addition to the solution just described, solutions were also obtained for Grashof numbers of 0.05, 1, 10, 50, 125 for a Prandtl number of 0.72; for Grashof numbers of 1250 and 12 500 for a Prandtl number of 10; and for a Grashof number of 50 for a Prandtl number of 100.

From the late-time steady-state solutions it was observed that even at extremely low Grashof numbers, weak convection processes were present in the region close to the outer boundary. However, it was found that even at moderate Grashof numbers the dominant mode of vorticity transport close to the surface of sphere was by diffusion. For all the solutions obtained it was observed that during the early stages of simulation the dominant mode of vorticity transport was by diffusion and that heat transfer took place largely by unsteady-state conduction. However, as integration proceeded with time the effects of convection increased until the late-time steady-state solutions were attained.

It was observed that the drag coefficients reached their late-time steady-state values more quickly than the other quantities and that the local Nusselt numbers took the longest time to reach their late-time steady-state values. For this reason the approach to the late-time steady-state condition was found to be best judged by observing the relative variation of the local Nusselt number with time. As the Grashof number was increased it was observed that the total time taken before late-time steady-state conditions were reached became shorter.

The main results of the present study are presented in Table 1. From this table it can be seen that as the Grashof number was increased it was found to be necessary to reduce the time-step, to increase the convergence criterion for the stream function and/or reduce the relaxation factor for the stream function. These changes were necessary in order to obtain convergence of the solution.

The main results obtained from the numerical solution of the steady-state equations [10] are presented in Table 2. As can be seen from a comparison of Tables 1 and 2, the results obtained from the solutions of the time-dependent and the time-independent equations are in reasonable agreement for Grashof numbers up to 25. However, as was explained [10], the solution for a Grashof number of 50 obtained from the steady-state equations is not reliable.

Based on the results obtained for average Nusselt numbers from this study and the previously mentioned time-independent study [10] the following relationships were developed:

$$Nu = 2 + 0.39\,(Ra)^{0.42} \tag{50}$$

for

$$0.05 \leqslant Gr < 50$$

$$Pr = 0.72$$

and

$$Nu = 2 + 0.75\,(Ra)^{0.25} \tag{51}$$

for

$$36 \leqslant Ra \leqslant 125\,000,$$

$$50 \leqslant Gr \leqslant 12\,500,$$

$$0.72 \leqslant Pr \leqslant 100.$$

Table 2. Main results of steady-state solution [10]

Gr	Pr	Nu	K_0	K_π	C_{DF}	C_{DP}
0.05	0.72	2.09	0.5	−0.40	1.17	0.58
1	0.72	2.39	5.97	−5.40	16.42	7.58
10	0.72	2.96	36.07	−31.26	74.88	71.29
25	0.72	3.32	76.23	−48.69	143.70	87.08
50	0.72	3.96	118.30	−12.66	211.20	105.45

Table 3. Comparison of average Nusselt numbers for different Grashof numbers for a Prandtl number of 0.72

Gr	Average Nusselt number, Nu, from ref. [ ]					
	Present study	[10]	[9]	[8]	[7]	[3]
0.05	2.1	2.09	2.32	2.43	2.18	2.05
1	2.34	2.39	2.67	2.90	2.54	
10	2.89	2.96	3.20		3.26	
25	3.31	3.32	3.51		3.73	
50	3.84	3.96	3.80		4.05	
125	4.31		4.26		4.59	
1250	6.11		6.03		6.60	
12 500	9.30		9.10		10.19	

Table 3 shows a comparison of the late-time steady-state values of the average Nusselt number obtained in the present study as predicted by relationships (50) and (51) with the results obtained by other workers from their analytical and experimental studies for a Prandtl number of 0.72. In this table the results obtained from the solutions of time-independent equations [10] are also included. It can be seen that the present solutions and the solutions of reference [10] predict lower values of the average Nusselt number than the experimental measurements. This could be because most experimental measurements of free convective heat transfer rates are influenced by disturbances in the fluid caused by external factors and suffer from losses due to conduction and radiation. These factors lead to overestimates of the average Nusselt numbers.

As stated earlier in this paper, the authors presented numerical solutions of steady-state free convective heat transfer from a solid sphere in the range of Grashof numbers between 0.05 and 50 [10]. However, as was explained in that paper, for a Grashof number of 50 the surface vorticity and, as a consequence, the surface pressure and the drag coefficients were slightly affected by the fluctuations of the vorticity at the outer boundary. To avoid numerical divergence of the surface vorticity, it was necessary to use much smaller relaxation factors and to increase the values of the convergence criteria. Even so, for Grashof numbers greater than 50, steady-state solutions could not be obtained. This was probably attributable to the steady-state method which was adopted in that study. Roache [16] has summarised the comparison between the iterative steady-state and time-dependent methods and concluded that the time-dependent method has proved to be generally more successful for viscous flow problems than the steady-state method. Since there is some confidence in the validity of the time-dependent equations of motion and energy, one is inclined to believe that a numerical solution which proceeds from a physically reasonable initial condition also has validity. Therefore, the success of the solution procedure developed in the present study may be attributed to the time-dependent approach which was adopted.

In the absence of mathematical analysis of the complete problem, which is not possible due to complexity of the set of interdependent partial differential equations describing free convective heat transfer from the surface of a sphere, the above arguments can never be confirmed but can only be contradicted if the solutions obtained are physically unrealistic. However, the solutions obtained were physically realistic and quantitatively reliable as far as could be ascertained from a comparison of the predicted results with existing data.

The solution procedure developed in this work has been used to obtain solutions for a restricted range of Grashof and Prandtl numbers and has also been applied to only one geometrical shape; the sphere. However, as procedure has been shown to provide reliable results, without particular difficulty, it could probably be used to obtain solutions for problems involving different geometries and different values of the Grashof and Prandtl numbers.

REFERENCES

1. J. J. Mahony, Heat transfer at small Grashof numbers, *Proc. R. Soc.* **A238,** 412–423 (1956).
2. F. E. Fendell, Laminar natural convection about an isothermally heated sphere at small Grashof numbers, *J. Fluid Mech.* **34,** 163–176 (1968).
3. M. A. Hossain, Laminar free convection about an isothermal sphere at extremely small Grashof numbers, Ph. D. Thesis, Cornell University (1966).
4. P. Mayer, Heat transfer to small Grashof particles by natural convection, *Instn Chem. Engrs* **15,** 127–130 (1937).
5. W. Elenbaas, The dissipation of heat by free convection from sphere and horizontal cylinders, *Physica* **9,** 285–296 (1942).
6. W. E. Ranz and W. R. Marshall Jr., Evaporation from drops, *Chem. Engng Prog.* **48,** 173–180 (1952).
7. W. G. Mathers, A. J. Madden, Jr and E. L. Piret, Simultaneous heat and mass transfer in free convection, *Ind. Engng Chem.* **49,** 961–968 (1957).
8. T. Tsubouchi and S. Sato, Heat transfer from fine wires and particles by natural convection, *Res. Inst. High Speed Mech. Tohoku University* **12,** 127–160 (1960).
9. T. Yuge, Experiments on heat transfer from spheres including combined natural and forced convection, *Trans. Am. Soc. Mech. Engrs.* Series C, *J. Heat Transfer* **82,** 214–220 (1960).
10. F. Geoola and A. R. H. Cornish, Numerical solution of steady-state free convective heat transfer from a solid sphere, *Int. J. Heat Mass Transfer* **24,** 1369–1379 (1981).
11. D. W. Peaceman and H. H. Rachford Jr., The numerical solution of parabolic and elliptic differential equations, *J. Soc. Ind. Appl. Math.* **3,** 28–41 (1955).

12. G. K. Batchelor, *An Introduction to Fluid Dynamics*, Chapters 2–5. Cambridge University Press (1970).
13. F. Geoola, Numerical simulation of free convective heat transfer from a sphere, Ph. D. Thesis, London University (1976).
14. G. D. Smith, *Numerical Solution of Partial Differential Equations*, Chapters 2 and 5. Oxford University Press, London (1965).
15. R. D. Richtmyer and K. W. Morton, *Difference Methods for Initial Value Problems*, (2nd edn) Chapter 1. John Wiley, New York (1967).
16. P. J. Roache, *Computational Fluid Dynamics*, Chapter 3. Hermosa, Albuquerque (1972).
17. J. S. Son and T. J. Hanratty, Numerical solution for flow around a cylinder at Reynolds numbers of 40, 200 and 500, *J. Fluid Mech.* **35**, 369–386 (1969).
18. K. Rafique, Digital simulation of viscous incompressible flow around a solid sphere, Ph.D. Thesis, London University (1971).
19. J. D. Hatim, Theoretical study of heat transfer from a solid sphere accelerating from rest, Ph.D. Thesis, London University (1975).
20. D. B. Spalding, A. D. Gosman and L. S. Caretto, Removal of an instability in a free convective problem, Ref. EF/TN/A/35 Mechanical Engineering Department Imperial College of Science and Technology, London (1971).
21. A. D. Gosman, W. W. Pun, A. K. Runchal, D. B. Spalding and M. Wolfshtein, *Heat and Mass Transfer in Recirculating Flow*. Academic Press, London (1969).
22. G. H. Bruce, D. W. Peaceman and H. H. Rachford, Jr., Calculations of unsteady-state gas flow through porous media, Petroleum *Trans. Am. Inst. Mech. Engrs* **198**, 79–92 (1953).
23. B. Carnahan, H. A. Luther and J. O. Wilkes, *Applied Numerical Methods*, Chapter 2. John Wiley, New York (1969).

Résumé—La convection libre du transfert de chaleur entre une sphère solide et un fluide Newtonien incompressible a été étudié numériquement pour des nombres de Grashof compris entre 0.05 et 12500 et pour des nombres de Prandtl égaux a 0.72, 10 et 100. Les équations de transport d'énergie et de tourbillon ont été résolues a l'aide de la méthode ADI de Peaceman et Rachford, et l'équation des fonctions de courant par une méthode ponctuelle d'itérations successives par relaxation. A l'aide des solutions stationnaires, on a observé des phénomènes de convection, même pour de très petits nombers de Grashof. De même, nous avons montré que la diffusion avait une large part au transport des tourbillons, même pour des nombres de Grashof assez importants.

NUMERISCHE SIMULATION VON WÄRMEÜBERTRAGUNGSVORGÄNGEN DURCH FREIE KONVEKTION AN EINER KUGEL

Zusammenfassung—Eine numerische Studie von zeitabhängigen Wärmeübertragungsvorgängen durch freie Konvektion zwischen einer festen Kugel und einem inkompressiblen Newton'schen Fluid wird für Grashof-Zahlen zwischen 0,05 und 12500 und für Prandtl-Zahlen von 0,71; 10 und 100 durchgeführt. Die Energie- und Wirbeltransportgleichungen wurden mit der ADI-Methode nach Peaceman und Rachford und die Stromfunktionsgleichung mit Hilfe der Überrelaxationsmethode gelöst. Aus der stationären Lösung war zu beobachten, daß auch bei sehr kleinen Grashof-Zahlen schwache Konvektionsvorgänge in der Zone nahe der äußeren Berandung auftraten. Es wurde jedoch gefunden, daß auch bei mittleren Grashof-Zahlen der Transport an der Oberfläche hauptsächlich durch Diffusion stattfand.

ЧИСЛЕННОЕ МОДЕЛИРОВАНИЕ СВОБОДНОКОНВЕКТИВНОГО ТЕПЛОПЕРЕНОСА ОТ СФЕРЫ

Аннотация—Выполнено численное исследование нестационарного свободноконвективного теплопереноса от твердой сферы к несжимаемой ньютоновской жидкости при значениях числа Грасгофа от 0,05 до 12500 и чисел Прандтля, равных 0,72; 10 и 100. Уравнения энергии и переноса вихрей решались методом переменных направлений Писмена и Рэчфорда, а уравнение функции тока–итерационным методом с использованием верхней релаксации. Согласно полученным в последнее время стационарным решениям уже при весьма малых значениях числа Грасгофа в области, прилегающей к внешней границе, имеют место слабые конвективные процессы. Однако, в данной работе показано, что даже при умеренных значениях числа Грасгофа перенос вихрей вблизи поверхности происходит в основном за счет диффузии.